

Int J Antimicrob Agents. 2020 Aug; 56(2): 106020.

PMCID: PMC7219429

Published online 2020 May 13. doi: [10.1016/j.ijantimicag.2020.106020](https://doi.org/10.1016/j.ijantimicag.2020.106020)

PMID: [32405156](https://pubmed.ncbi.nlm.nih.gov/32405156/)

Synergistic antiviral effect of hydroxychloroquine and azithromycin in combination against SARS-CoV-2: What molecular dynamics studies of virus-host interactions reveal

Jacques Fantini,^{a,*} Henri Chahinian,^b and Nouara Yahi^b

^aINSERM UMR_S 1072, 13015 Marseille, France

^bAix-Marseille Université, 13015 Marseille, France

*Corresponding author.

Received 2020 Apr 3; Accepted 2020 May 4.

[Copyright](#) © 2020 Elsevier B.V. and International Society of Chemotherapy. All rights reserved.

Since January 2020 Elsevier has created a COVID-19 resource centre with free information in English and Mandarin on the novel coronavirus COVID-19. The COVID-19 resource centre is hosted on Elsevier Connect, the company's public news and information website. Elsevier hereby grants permission to make all its COVID-19-related research that is available on the COVID-19 resource centre - including this research content - immediately available in PubMed Central and other publicly funded repositories, such as the WHO COVID database with rights for unrestricted research re-use and analyses in any form or by any means with acknowledgement of the original source. These permissions are granted for free by Elsevier for as long as the COVID-19 resource centre remains active.

Abstract

The emergence of SARS-coronavirus-2 (SARS-CoV-2) has led to a global pandemic disease referred to as coronavirus disease 19 (COVID-19). Hydroxychloroquine (CLQ-OH)/azithromycin (ATM) combination therapy is currently being tested for the treatment of COVID-19, with promising results. However, the molecular mechanism of action of this combination is not yet established. Using molecular dynamics (MD) simulations, this study shows that the drugs act in synergy to prevent any close contact between the virus and the plasma membrane of host cells. Unexpected molecular similarity is shown between ATM and the sugar moiety of GM1, a lipid raft ganglioside acting as a host attachment cofactor for respiratory viruses. Due to this mimicry, ATM interacts with the ganglioside-binding domain of SARS-CoV-2 spike protein. This binding site shared by ATM and GM1 displays a conserved amino acid triad Q-134/F-135/N-137 located at the tip of the spike protein. CLQ-OH molecules are shown to saturate virus attachment sites on gangliosides in the vicinity of the primary coronavirus receptor, angiotensin-converting enzyme-2 (ACE-2). Taken together, these data show that ATM is directed against the virus, whereas CLQ-OH is directed against cellular attachment cofactors. We conclude that both drugs act as competitive inhibitors of SARS-CoV-2 attachment to the host-cell membrane. This is consistent with a synergistic antiviral mechanism at the plasma membrane level, where therapeutic intervention is likely to be most efficient. This molecular mechanism may explain the beneficial effects of CLQ-OH/ATM combination therapy in patients with COVID-19. Incidentally, the data also indicate that the conserved Q-134/F-135/N-137 triad could be considered as a target for vaccine strategies.

Keywords: Coronavirus, Pandemic, SARS-CoV-2, Ganglioside, Azithromycin, Chloroquine

Abbreviations: ACE-2, angiotensin-converting enzyme-2; ATM, azithromycin; CLQ, chloroquine; CLQ-OH, hydroxychloroquine; COVID-19, coronavirus disease 19; NTD, N-terminal domain; RBD,

receptor binding domain; SARS-CoV, severe acute respiratory syndrome coronavirus; SARS-CoV-2, SARS-coronavirus-2

1. Introduction

The emergence of the novel pathogenic SARS-coronavirus 2 (SARS-CoV-2) has led to a global pandemic disease referred to as coronavirus disease 19 (COVID-19) [1]. In such a health emergency, it is critical to find a cure and stop the pandemic. Among the potential solutions currently under investigation, a combination bitherapy consisting of the antimalarial drug, hydroxychloroquine (CLQ-OH) with the antibiotic, azithromycin (ATM) has received particular attention. Following initial reports from China indicating a potential effect of chloroquine (CLQ) [2], a preliminary clinical trial was implemented in France on a small cohort of COVID-19 patients [3]. A significant viral load reduction was observed in the 20 patients treated with CLQ-OH [3], a CLQ derivative with increased solubility in water and decreased toxicity [4]. With the aim of preventing bacterial super-infection, six additional patients in this trial also received ATM for 5 days. All these patients had undetectable viral load after 6 days [3]. Thus, although these promising data need clinical confirmation with more patients, CLQ-OH/ATM combination therapy already appears superior to CLQ alone as a first-line treatment for COVID-19.

Both CLQ-OH and ATM are repositioned drugs and their antiviral mechanism of action, particularly in combination, remains mostly unclear. In vitro studies have shown that CLQ-OH inhibits SARS-CoV-2 [4, 5, 6]. Far less is known about the antiviral effects of ATM, which has been suggested to interfere with influenza virus internalization [7]. Interestingly, CLQ is also considered as an inhibitor of endocytic pathways through an elevation of endosomal pH [8]. However, several reports indicate that CLQ could also prevent virus attachment through a direct effect on host-cell surface molecules [9,10].

The first step of the replication cycle in human coronaviruses is the attachment of the virus to the host plasma membrane, which is mediated by a membrane protein receptor, i.e., angiotensin-converting enzyme-2 (ACE-2) in the case of SARS-CoV-2 [11]. Moreover, coronaviruses are also dependent upon sialylated membrane components, such as gangliosides, which act as attachment cofactors within lipid raft membrane platforms [12, 13, 14]. As ACE-2 is localized in lipid rafts [15], SARS-CoV-2 infection requires specific targeting to these plasma membrane microdomains, where multivalent interactions between the spike protein and raft components can take place. In line with this notion, lipid raft disruption through cholesterol depletion resulted in a significant reduction of human coronavirus SARS-CoV infection [15]. The recent identification of a potential ganglioside-binding domain in the N-terminal domain (NTD) of the SARS-CoV-2 spike protein, and its potential role in membrane recognition [10], prompted this study of the molecular relationship between this domain, gangliosides, ATM and CLQ-OH. This study involved a molecular modelling strategy that has been successfully applied to unravel the molecular mechanisms of protein binding to raft lipid components, including gangliosides [16,17] and cholesterol [18,19].

2. Materials and Methods

2.1. Pdb files

The SARS-CoV-2 spike protein trimer in the prefusion conformation was obtained from pdb file # 6VSB [20]. Hydroxychloroquine (CLQ-OH) is (RS)-2-[[4-[(7-chloroquinolin-4-yl)amino]pentyl](ethyl)amino]ethanol. CLQ-OH was generated by hydroxylation of chloroquine (CLQ) and validated as previously described [10]. CLQ was retrieved from pdb file # 4V2O (CLQ co-crystallized with saposin B) [21].

Azithromycin (ATM) is (2R,3S,4R,5R,8R,10R,11R,12S,13S,14R)-11-[(2S,3R,4S,6R)-4-(dimethylamino)-3-hydroxy-6-methyloxan-2-yl]oxy-2-ethyl-3,4,10-trihydroxy-13-[(2R,4R,5S,6S)-5-hydroxy-4-methoxy-4,6-dimethyloxan-2-yl]oxy-3,5,6,8,10,12,14-heptamethyl-1-oxa-6-azacyclopentadecan-15-one. The 3D structure of ATM was obtained from pdb file # 5UXD (ATM co-crystallized with macrolide 2'-phosphotransferase) [22].

2.2. Molecular modelling and visualization tools

Molecular modelling studies were performed using Hyperchem (<http://www.hyper.com>), Deep View/Swiss-Pdb viewer (<https://spdbv.vital-it.ch>) and Molegro Molecular viewer (<http://molexus.io/molegro-molecular-viewer>) as described previously [16, 17, 18, 19, 23]. Lennard-Jones parameters and atomic charges of ATM obtained from pdb file # 5UXD were checked with Hyperchem. The molecular modelling protocol consisted of docking, equilibration, and subsequent 50-ns molecular dynamics (MD) simulations with CHARMM force field [16, 24] in Hyperchem. The starting point for ATM docking was done by manual positioning on the NTD and receptor-binding domain (RBD) surfaces of SARS-CoV-2 spike protein (chain A) with full consideration of the properties of the drug. In addition, a series of 20 randomly positioned ATM molecules covering the whole NTD surface were analysed. Energy minimization of each system was then performed with the Polak-Ribière conjugate gradient algorithm, with CHARMM force field in Hyperchem, using a maximum of 3×10^5 steps, and a root-mean-square (RMS) gradient of $0.01 \text{ kcal} \cdot \text{Å}^{-1} \cdot \text{mol}^{-1}$ as the convergence condition. According to the validation ligand-binding protocol [25], the optimized docked structures were used as the initial structures for MD simulations with the following parameters: heat time 5 ps, run time 10 ps, step size 1 fs, starting temperature 0 K, simulation temperature 300 K, temperature step 30 K, bath relaxation time step size 0.1 ps. Each complex was submitted to 50-ns long MD trajectories, replicated three times, with convergent trajectories obtained. Frames were saved at 10 ns intervals for subsequent analysis. The final complex obtained with chain A was reintroduced in the trimeric spike structure (pdb file # 6VSB) with Molegro Molecular viewer and with Deep View Swiss-Pdb viewer. Similar results were obtained with both programs. The energies of interaction were extracted from the Ligand Energy Inspector function of Molegro Molecular viewer. Molecular volumes were calculated by the QSAR function of Hyperchem.

2.3. Ganglioside GM1

The initial coordinates of ganglioside GM1 were obtained from CHARMM-GUI Glycolipid Modeler [24] (<http://www.charmmgui.org/?doc=input/glycolipid>), which uses the internal coordinate information of common glycosidic torsion angle values, orientates the ganglioside perpendicular to the membrane, and performs Langevin dynamics with a cylindrical restraint potential to keep the whole GM1 molecule cylindrical, particularly the membrane-embedded ceramide part. In the next step, the saccharide part of the ganglioside was included in a periodic box solvated with 1128 water molecules (dimensions: 34848 Å^3 with $x = 33 \text{ Å}$, $y = 32 \text{ Å}$, $z = 33 \text{ Å}$). The system was energy-minimized 6 times switching alternatively between runs using steepest descent gradients or Polak-Ribière conjugate gradients until convergence to machine precision [16]. The dimer of ganglioside GM1 interacting with 4 CLQ-OH molecules was obtained by MD simulations of a previously described model [10]. To mimic GM1 gangliosides in a typical lipid raft membrane domain, two GM1 molecules were merged with eight cholesterol and two sphingomyelin lipids. The whole system was optimized, merged with SARS-CoV-2 spike protein (chain A) and submitted to MD simulations with the same conditions as those used for the ATM-spike protein complex (50-ns run in triplicate). For comparison, similar MD simulations were performed on an isolated GM1 dimer in the CHARMM-GUI membrane-compatible topology but without surrounding lipids.

3. Results

3.1. Molecular mimicry between ATM and ganglioside GM1

The chemical structure of ATM is shown in Fig. 1 a. The molecule contains two sugar-like pyranil rings, one with a nitrogen-containing group (N-pyr), the other with an acetyl group (Ac-pyr). The remaining part of the molecule is cyclic, so that its overall conformational flexibility, although significant, is restricted to a limited spatial volume of 2082 Å^3 (Fig. 1b). Interestingly, this volume is almost the same as that of the saccharide part of ganglioside GM1 (2293 Å^3 , Fig. 1b), a lipid raft ganglioside that plays a critical role in the binding and endocytosis of respiratory viruses [26], including pathogenic human coronaviruses [27]. Beyond their similar spatial volume, the saccharide part of GM1 and ATM also share some analogous chemical features, including sugar rings and a solvent-accessible

surface dotted with several CH and OH groups (Fig. 1b). This molecular similarity is further illustrated in Figure S1 where ATM is superimposed on the saccharide part of GM1.

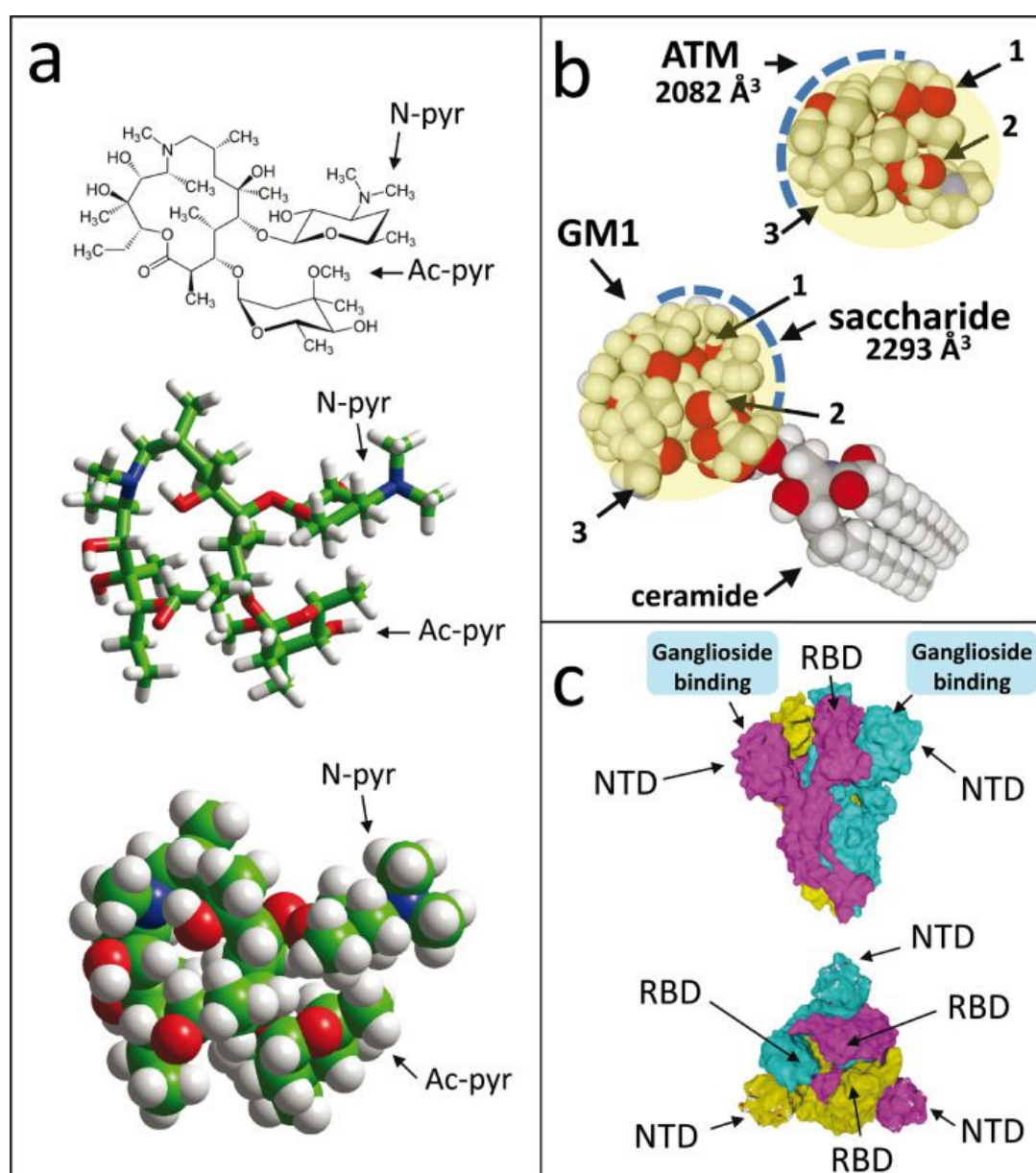


[Fig. 1](#)

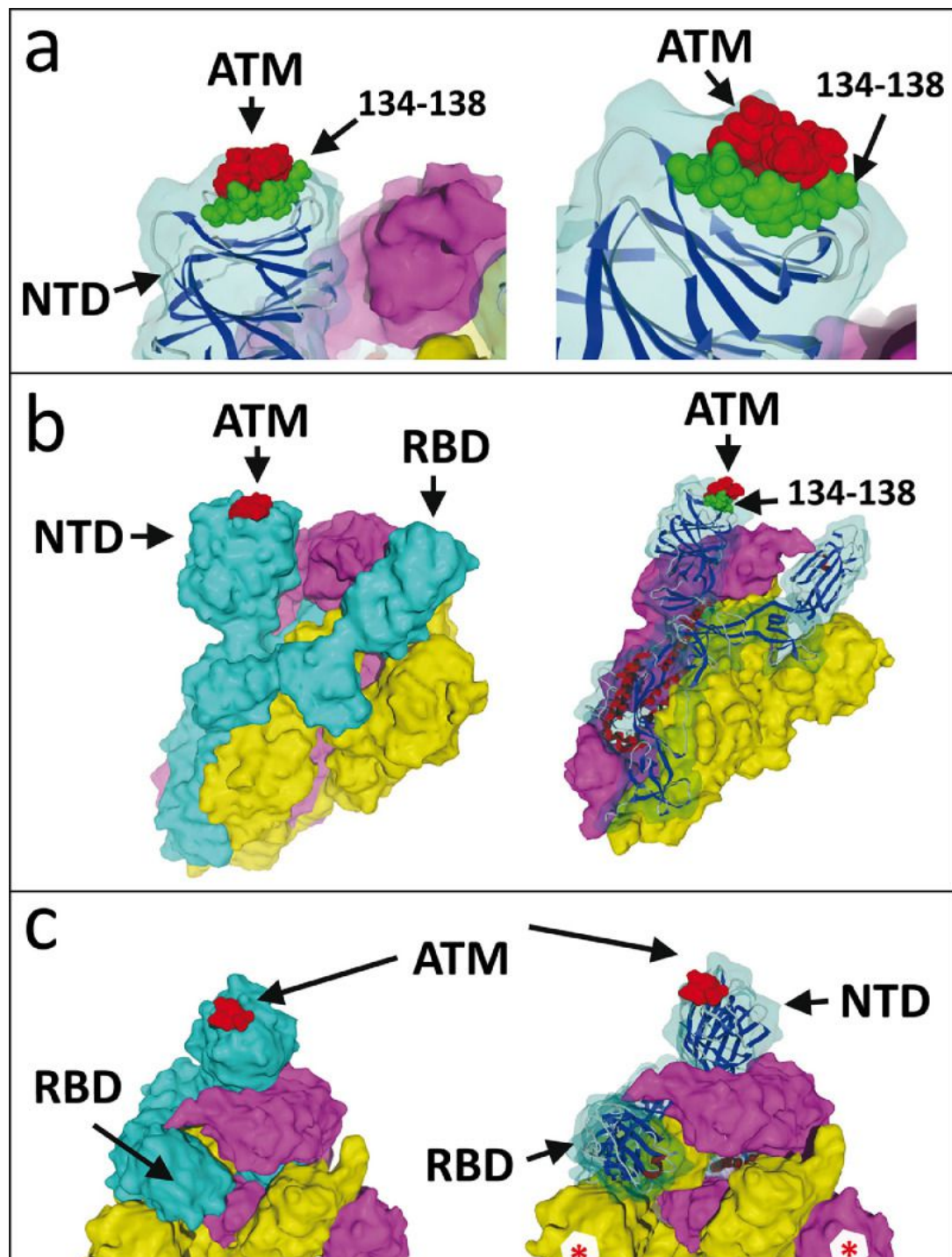
[Open in a separate window](#)

Structures of azithromycin (ATM) and SARS-CoV-2 spike protein trimer. (a) ATM, with both sugar-like pyranil groups N-pyr and Ac-pyr indicated. The molecules are shown in chemical, tube and sphere rendering (carbon in green, nitrogen in blue, oxygen in red, hydrogen in white). (b) Molecular structure similarity between ATM and the saccharide part of ganglioside GM1. Both structures can adopt a globular shape the surface of which is covered with a patchwork of OH (arrows 1 and 2) and CH groups (arrow 3). The volume occupied by ATM and the saccharide part of GM1 can be estimated to be 2082 and 2293 Å³, respectively. (c) front and above views of the trimeric spike, each spike protein subunit with a distinct surface colour (cyan for chain A, yellow for chain B, purple for chain C). Atoms belonging to the ganglioside-binding domain of each subunit are visible underneath the slightly transparent surface. The ganglioside-binding domains, the NTD and the RBD are indicated.

Given that the SARS-CoV-2 spike protein displays a ganglioside-binding site at the tip of its NTD [10], the possibility that ATM, as a “ganglioside mimic”, could also bind to this site was considered. The structural features of the SARS-CoV-2 spike in the prefusion conformation [20] are shown in Fig. 1c. It consists of three interdigitated spike proteins that provide the virus its typical corona-like shape in electron microscopy images. In each subunit, the most distant part from the viral envelope is divided into two separate domains, the NTD and the RBD. The NTD has a flat surface available for ganglioside binding [10], and this process is independent from the ACE-2 receptor recognition, which occurs at the tip of the RBD [11,20]. When seen from above, the viral spike has a typical triangle shape, with a ganglioside-binding domain at each apex. Thus, the spike central area is devoted to ACE-2 binding, leaving three peripheric flat surface areas available for ganglioside attachment. Such dual ganglioside/receptor binding is commonly used by pathogenic viruses such as HIV-1 [28], [29], [30] and bacterial neurotoxins [16]. By combining the high affinity for a single protein receptor with multiple low affinity attachment sites, these pathogens have selected a very efficient pathway to gain entry into host cells.

3.2. Characterization of an ATM binding site at the tip of SARS-CoV-2 spike protein

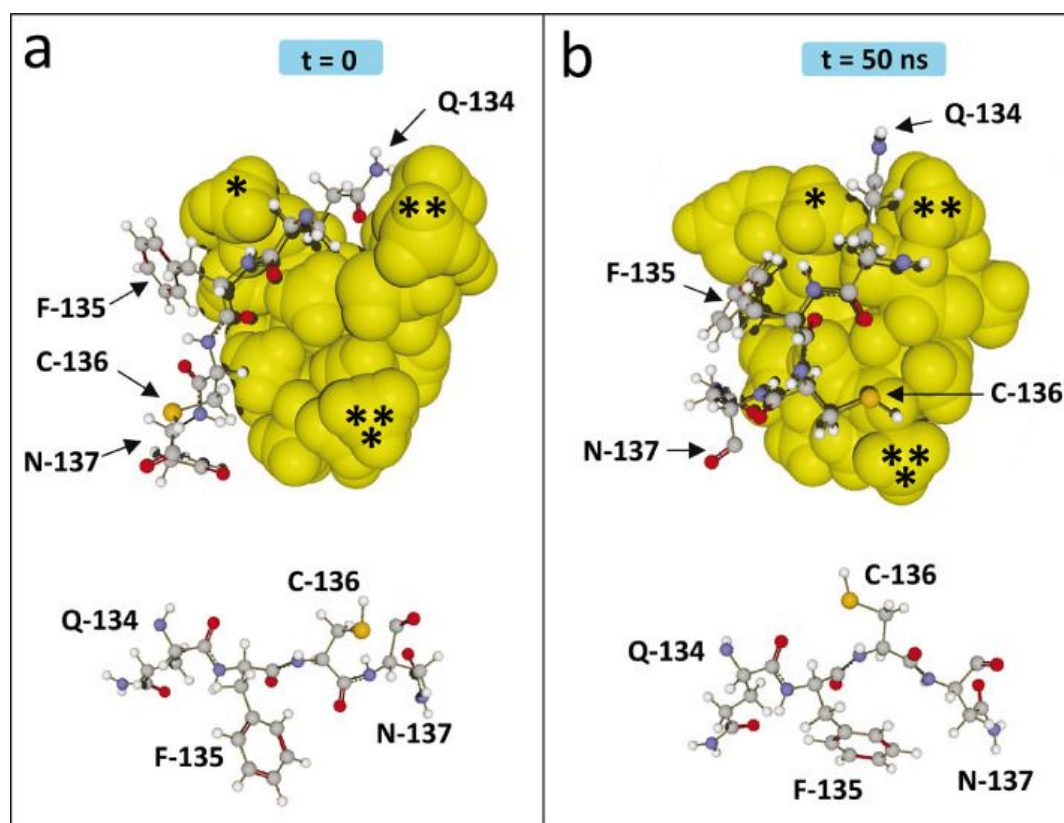
When ATM molecules were merged with the SARS-CoV-2 spike protein, there was a very good fit for one particular pose at the tip of protein (Fig. 2). All other docking attempts on the NTD or the RBD of the spike protein were unsuccessful (Figure S2) as they did not satisfy the minimum cut-off values. Not surprisingly, their trajectories started destabilizing before 10 ns. In contrast, ATM #1 (coloured in yellow in Figure S2) remained bound to the spike protein throughout the simulation process (Fig. 3). Interestingly, a significant movement of the drug was observed from its docked pose to a stable MD pose (dock-to-MD transition), particularly during the first 10-ns of simulations (Figure S3). A stable complex association was then reached after 10 ns. Three amino acid residues, referred to as the “QFN triad”, exhibited significant conformational rearrangement during the binding process: Q-134, F-135 and N-137 (Fig. 3). The principal moves comprised a significant reorientation of the aromatic ring of F-135, from suboptimal stacking to stabilized T-shape CH- π interaction, and a concomitant retraction of the Q-134 side chain. Fluctuations during the 10 to 50 ns period did not affect the overall geometry of the complex, which converged to a mean energy of interaction of $92.4 \pm 5.8 \text{ kJ.mol}^{-1}$ as determined from triplicate MD simulations (Table S1). Schematically, the binding site is formed by two discontinuous regions of the protein, including the QFN triad with additional C-136, D-138, R-158 and S-161 residues (Fig. 4, Fig. 5). These seven amino acid residues accounted for almost 90% of the whole energy of interaction (Table S1 and Fig. 5).



[Open in a separate window](#)

Fig. 2

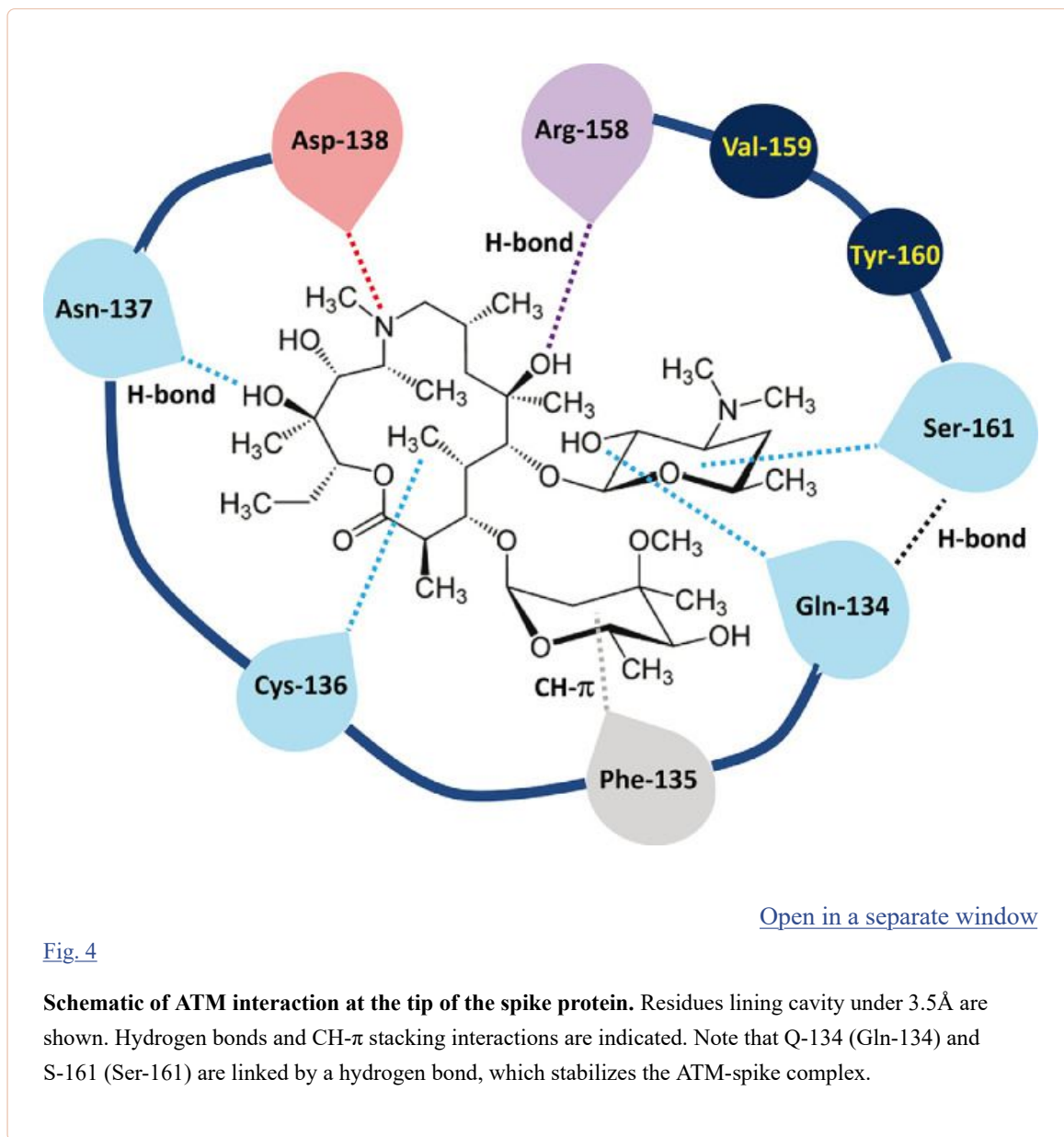
Molecular complex between the SARS-CoV-2 spike protein trimer and ATM. (a) Detailed view of ATM bound to the NTD tip of SARS-CoV-2 spike protein chain A, shown at two distinct magnifications and orientations (left and right panels). Note that the NTD tip displays a complementary landing surface for ATM (highlighted in red). The protein stretch 134-138, which contains the QFN triad, is highlighted in green. (b) The trimeric structure of the SARS-CoV-2 spike is represented in surface rendition with subunit (protein chain A, B and C) in cyan, yellow and purple, respectively. AMT (in red) is bound to the tip of the NTD domain of the A subunit (left panel). The ribbon structure of the cyan (chain A) subunit is shown in the right panel. (c) Above views of the spike-ATM complex. Note that the B and C subunits also display a fully accessible ATM binding site (red asterisk).

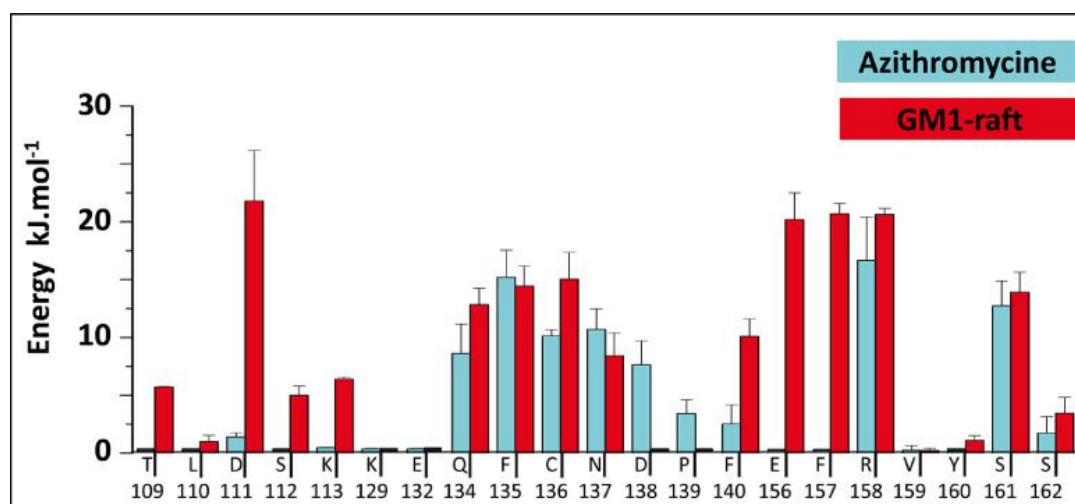


[Open in a separate window](#)

[Fig. 3](#)

Induced-fit conformational rearrangements during binding of ATM on the spike protein. (a) Docking of ATM on the spike protein (time = 0). ATM is in yellow spheres, and the protein segment 134-137 is in balls and sticks rendition. Three parts of the ATM molecule are marked with asterisks. The orientation of the side chains of residues 134-137 is shown under the complex. (b) ATM bound to the spike protein after MD simulations (time = 50 ns). Note that the complex has evolved according to a typical induced-fit mechanism. The asterisks on ATM help visualize its conformational changes. Reorientation of amino acid side chains is also clearly visible in the ATM-spike complex and in the isolated 134-137 fragment shown under the complex.





[Open in a separate window](#)

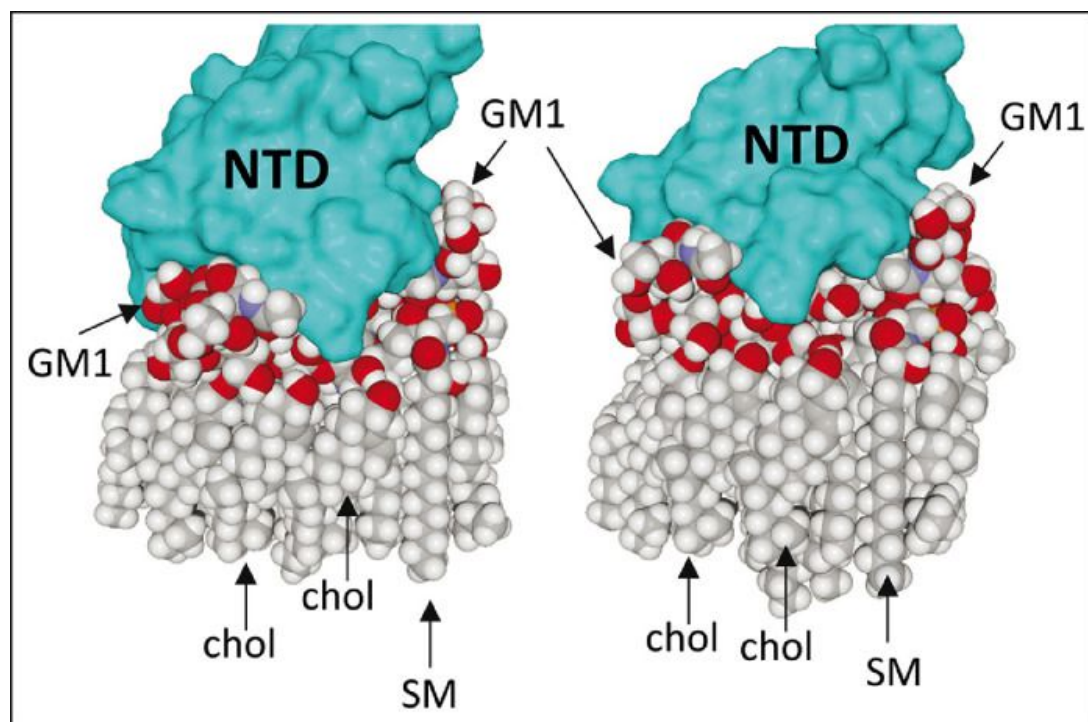
Fig. 5

Energy of interaction of spike protein-ATM and spike-GM1 complexes. Results are expressed by amino acid residue as mean \pm SD of three distinct MD simulations (50 ns) with the same starting docking conditions. In the case of GM1, the simulations are done in presence of sphingomyelin and cholesterol to mimic a lipid raft plasma membrane domain. Each bar corresponds to a single amino acid residue, as indicated in the horizontal axis. Detailed values and statistics are shown in Table S1.

The complex was stabilized by hydrogen bonds, CH- π and van der Waals interactions distributed over the whole ATM molecule (Fig. 4).

3.3. SARS-CoV-2 spike protein interactions with gangliosides in a lipid raft domain

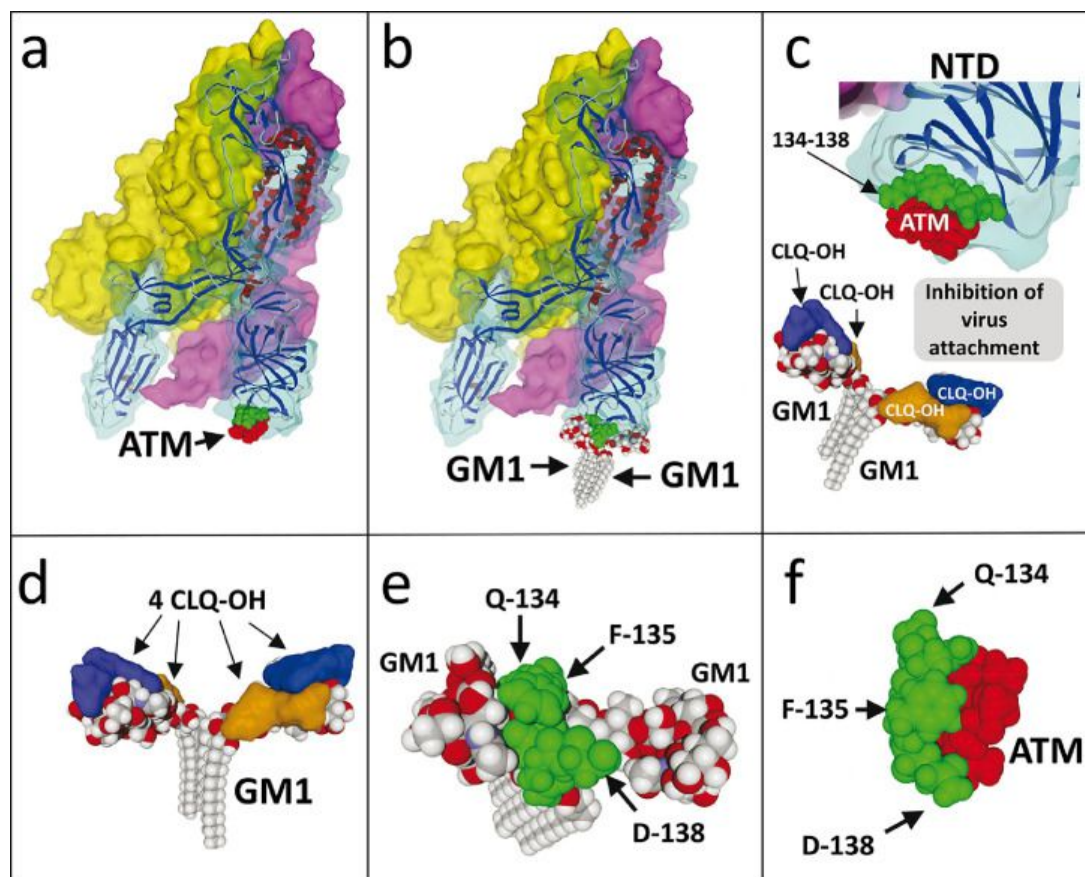
Based on recent in-silico data that led to the characterization of ganglioside-spike protein interactions [10], MD simulations were performed with GM1 gangliosides surrounded by typical raft lipids, i.e. sphingomyelin and cholesterol (Figs. 5 and 6). These new data confirmed and extended our previous results obtained with isolated gangliosides [10]. Indeed, cholesterol and sphingomyelin appeared to stabilize the typical chalice-shaped GM1 dimer, which serves as a landing platform for the SARS-CoV-2 spike protein (Fig. 6). Moreover, the histograms of Fig. 5 show that all amino acid residues of the spike protein that are involved in ATM binding, including the QFN triad, are also essential for GM1 binding in the lipid raft environment (Table S1 and Fig. 5). Taken together, these data indicate that the NTD of the viral glycoprotein may display a common ganglioside/ATM binding site, in agreement with our working hypothesis. Sequence alignments revealed that this common binding site, including the QFN triad, is totally conserved among clinical isolates of SARS-CoV-2 from various geographical origins worldwide (Fig. 7). It is also conserved in bat RaTG13, which further illustrates the close relationship between this bat coronavirus and the SARS-CoV-2 strains that are currently circulating the world. This region of the NTD should therefore be considered for SARS-CoV-2 vaccine strategies. However, the motif has a different sequence signature in other animal- and human-related SARS coronaviruses (Fig. 7), indicating a recent evolution that may be linked to the higher contagiousness of SARS-CoV-2 compared with other human coronaviruses.



[Open in a separate window](#)

Fig. 6

MD simulations of GM1-spike protein interaction in a lipid raft domain. Two GM1 gangliosides were merged with eight cholesterol (chol) and two sphingomyelin (SM) lipids. After initial docking, MD simulations were performed for 50 ns. Two distinct views of the complex are shown. Cholesterol and sphingomyelin stabilize a dimer of GM1 clamped by the NTD of the spike protein.



[Open in a separate window](#)

Fig. 8

CLQ-OH/ATM combination therapy at the molecular level. (a) ATM bound to the SARS-CoV-2 spike protein trimer. (b) Ganglioside dimer (two symmetrically arranged GM1 molecules in a typical chalice-like shape, just like the one observed in lipid raft simulations) bound to SARS-CoV-2 spike protein trimer. Note that both ATM and gangliosides share the same binding region. (c) ATM prevents ganglioside binding to the SARS-CoV-2 spike protein trimer. CLQ-OH, once bound to gangliosides (blue and orange surfaces), also prevents any interaction with the viral spike. (d) 4 CLQ-OH molecules bound to a ganglioside dimer. Each GM1 molecule is blocked by two CLQ-OH molecules (blue and orange surfaces), which wrap around the saccharide part. (e) Detail of the 134-138 SARS-CoV-2 spike protein stretch bound to GM1. Note that the ganglioside interacts with Q-134 and F-135, but not with D-138. (f) Detail of the 134-138 SARS-CoV-2 spike protein stretch bound to ATM. In this case, the binding site includes D-138 in addition to Q-134 and F-135. Note that N-137, which interacts with both ATM and GM1, is not visible in these representations as it is located behind.

This study also looked at CLQ-OH and its interaction with GM1. We recently published a model describing a complex formed by one GM1 and two CLQ-OH molecules [10]. For comparison, the same molecular modelling approaches as for ATM (in the presence of surrounding raft lipids) were applied to this model. A stable complex formed by a ganglioside dimer, each monomer being associated with two CLQ-OH molecules, was obtained (Fig. 8d). The stability of this complex is reinforced by a rearrangement of CLQ-OH molecules that interact with each other as well as interacting with the saccharide part of GM1. Consequently, the surface of the ganglioside is almost completely masked, so that the ganglioside dimer can no longer be recognized by the viral spike (Fig. 8c). In the presence of both ATM and CLQ-OH, virus-ganglioside interactions are efficiently blocked, preventing any close contact between the virus and the plasma membrane of host cells. The molecular details of this

synergistic antiviral effect are worth mentioning. As shown in [Figs. 5](#) and [8e](#) and Table S1, the QFN triad of the virus spike protein is predicted to interact with the central region of the ganglioside dimer. If the dimer is compared metaphorically to a butterfly, this region corresponds to the insect's head between the wings. For its part, CLQ-OH binds to the wings ([Fig. 8d](#)), whereas ATM neutralizes the QFN triad of the virus spike protein ([Fig. 8f](#)). Indeed, all attempts to obtain a stable raft-spike protein complex aborted when GM1 was covered by CLMQ-OH and when ATM was bound to the spike protein. In the case of ATM, these data confirm that the QFN triad is critical for GM1 recognition and that although other residues are involved ([Fig. 5](#) and Table S1), the whole binding process is fully controlled by the primary interaction driven by the QFN triad. In agreement with this notion, mutating the QFN triad with alanine residues resulted in an aborted ATM binding process at the post-docking steps. Taken together, these molecular modelling studies indicate that CLQ-OH and ATM, when bound to their respective targets, totally mask the complementary surfaces provided by the lipid raft and the virus spike ([Fig. 8c](#)): CLQ-OH binds to GM1 and covers the wing, ATM binds to the virus spike and prevents any interaction with the central area of the ganglioside dimer. Hence, both drugs act as competitive inhibitors of SARS-CoV-2 attachment to the host-cell membrane.

4. Discussion

In this study, molecular modelling approaches specifically dedicated to virus-host interactions were used to unravel the antiviral mechanism of action of ATM and CLQ-OH in combination. The study method included a first round of molecular docking, followed by MD simulations of protein-ligand interactions to assess the robustness of each model [\[25\]](#). Such computer-assisted simulations are particularly helpful for studying protein-ganglioside interactions as crystallographic approaches are usually limited to the water-soluble saccharide part of the ganglioside, neglecting the membrane embedded-ceramide part [\[31\]](#). Unfortunately, the ceramide moiety of gangliosides has a marked effect on the saccharide part with which it interacts, resulting in significant restriction of its conformational possibilities [\[32\]](#). Therefore, data obtained with oligosaccharides cannot be systematically transposed to intact gangliosides. Molecular modelling approaches circumvented this difficulty and enabled study of whole gangliosides in membrane-compatible conformations [\[16,32,33\]](#). The MD simulations performed in the present study were done on gangliosides surrounded by cholesterol and sphingomyelin, which mimic a lipid raft environment.

To date, there are several structural data of the SARS-CoV-2 protein in the prefusion conformation or bound to its primary receptor ACE-2 [\[11, 20\]](#). However, ACE-2 is in lipid rafts and raft disruption induces a marked decrease of virus infection [\[15\]](#). Thus, it is likely that the virus interacts with the raft surface through multivalent contacts involving both ACE-2 and gangliosides. The fact that the RBD and the ganglioside-binding domain belong to distinct parts of the trimeric spike is consistent with this notion. Such a complex network of virus-host cell membrane interactions is also consistent with previously characterized virus infection strategies. Indeed, the HIV-1 fusion process driven by gp120 and gp41 envelope proteins involves a receptor (CD4), a coreceptor (chiefly CCR5) and glycosphingolipid cofactors [\[39\]](#). Like SARS-CoV-2, the pentameric capsid protein of SV40, and polyoma viruses display three distinct binding sites for gangliosides, which serve as critical receptors for these non-enveloped viruses in lipid raft domains [\[40\]](#).

The MD simulations in the current study indicate that both CLQ-OH and ATM may block SARS-CoV2 binding to gangliosides via mirror competitive mechanisms. ATM, which has some molecular similarity with GM1 sugar, can thus occupy the ganglioside-binding domain of the spike protein and neutralize virus binding to lipid rafts. CLQ-OH covers the ganglioside surface, and thus also prevents virus-membrane interaction through a complementary mechanism. Each of these drugs might be efficient alone to block virus attachment, ATM through virus binding, CLQ-OH through ganglioside binding. As both drugs interfere with the same mechanism but with distinct molecular targets, they are expected to work together in synergy, as indicated by recent clinical data [\[3\]](#).

The posology of the combination therapy for COVID-19 is 600 mg CLQ-OH and 250 mg ATM per day [\[3,34\]](#). This ratio corresponds to a molar ratio of five CLQ-OH for one ATM. In silico calculations

indicate a binding ratio of four CLQ-OH for one ATM, which is close to the posology. Furthermore, as ATM shares structural similarity with the saccharide part of GM1, one should ask whether ATM could bind to CLQ-OH and by this way reduce the potential effectiveness of this combination therapy. However, as ATM and CLQ-OH have been reported to synergistically decrease SARS-CoV-2 load in infected patients [3], drug cross-neutralization is very unlikely. There was a consistent lack of evidence of any stable ATM-CLQ-OH complexes using the molecular modelling approaches in this study.

The molecular mimicry between ATM and the saccharide part of GM1 gives new perspectives on the therapeutic effect of this macrolide antibiotic and this warrants further exploration. Moreover, the fact that ganglioside GM1 is a molecular target for CLQ-OH might explain the indication of this drug in rheumatological disorders, such as lupus and rheumatoid arthritis [35,36]. Indeed, GM1 overexpression and anti-GM1 antibodies are a hallmark of these diseases [37,38]. Thus, our data incidentally indicate that the therapeutic effect of CLQ-OH in these cases could also be related to its ganglioside-binding properties.

5. Conclusion

In conclusion, ATM and CLQ-OH have synergistic antiviral effects on SARS-CoV-2 infection, which supports the use of this combination therapy for the COVID-19 pandemic. In this bitherapy, one molecule (ATM) is directed against the virus, while the other (CLQ-OH) is directed against cellular attachment cofactors. However, the two drugs are predicted to act in synergy to prevent the first step of SARS-CoV-2 infection, at the plasma membrane level, where therapeutic intervention is likely to be most efficient. The conserved QFN triad of the SARS-CoV-2 spike protein, which is recognized by both gangliosides and ATM, should be considered as a target for neutralizing antibodies in vaccine strategies. The molecular modelling approaches used here are based on the search for ganglioside saccharide mimicry and might be useful to identify other ATM binding sites on virus proteins, and more generally to predict the efficacy of any potential repurposed and/or innovative drug candidates before clinical evaluation. In this respect, we suggest testing the antiviral association of ATM with short synthetic peptides specifically designed to target gangliosides without toxicity [17,33].

Declarations

Funding

None

Competing Interests

None.

Ethical Approval

Not required.

Footnotes

Funding: This research did not receive any specific grant from funding agencies in the public, commercial, or not-for-profit sectors.

Supplementary material associated with this article can be found, in the online version, at [doi:10.1016/j.ijantimicag.2020.106020](https://doi.org/10.1016/j.ijantimicag.2020.106020).

Appendix. Supplementary materials

[Click here to view.](#) (1.3M, pdf) Image, application 1

References

1. Wu F, Zhao S, Yu B, Chen YM, Wang W, Song ZG. A new coronavirus associated with human respiratory disease in China. *Nature*. 2020;579:265–269. doi: 10.1038/s41586-020-2008-3. [[PMC free article](#)] [[PubMed](#)] [[CrossRef](#)] [[Google Scholar](#)]
2. Gao J, Tian Z, Yang X. Breakthrough: Chloroquine phosphate has shown apparent efficacy in treatment of COVID-19 associated pneumonia in clinical studies. *Biosci Trends*. 2020;14:72–73. doi: 10.5582/bst.2020.01047. [[PubMed](#)] [[CrossRef](#)] [[Google Scholar](#)]
3. Gautret P, Lagier JC, Parola P, Hoang VT, Meddeb L, Mailhe M. Hydroxychloroquine and azithromycin as a treatment of COVID-19: results of an open-label non-randomized clinical trial. *Int J Antimicrob Agents*. 2020;20 doi: 10.1016/j.ijantimicag.2020.105949. [[PMC free article](#)] [[PubMed](#)] [[CrossRef](#)] [[Google Scholar](#)]
4. Liu J, Cao R, Xu M, Wang X, Zhang H, Hu H. Hydroxychloroquine, a less toxic derivative of chloroquine, is effective in inhibiting SARS-CoV-2 infection in vitro. *Cell Discov*. 2020;6:16. doi: 10.1038/s41421-020-0156-0. [[PMC free article](#)] [[PubMed](#)] [[CrossRef](#)] [[Google Scholar](#)]
5. Yao X, Ye F, Zhang M, Cui C, Huang B, Niu P. In vitro antiviral activity and projection of optimized dosing design of hydroxychloroquine for the treatment of Severe Acute Respiratory Syndrome Coronavirus 2 (SARS-CoV-2) *Clin Infect Dis*. 2020 doi: 10.1093/cid/ciaa237. pii:ciaa237. [[PMC free article](#)] [[PubMed](#)] [[CrossRef](#)] [[Google Scholar](#)]
6. Wang M, Cao R, Zhang L, Yang X, Liu J, Xu M. Remdesivir and chloroquine effectively inhibit the recently emerged novel coronavirus (2019-nCoV) in vitro. *Cell Res*. 2020;30:269–271. doi: 10.1038/s41422-020-0282-0. [[PMC free article](#)] [[PubMed](#)] [[CrossRef](#)] [[Google Scholar](#)]
7. Tran DH, Sugamata R, Hirose T, Suzuki S, Noguchi Y, Sugawara A. Azithromycin, a 15-membered macrolide antibiotic, inhibits influenza A(H1N1)pdm09 virus infection by interfering with virus internalization process. *J Antibiot (Tokyo)* 2019;72:759–768. doi: 10.1038/s41429-019-0204-x. [[PubMed](#)] [[CrossRef](#)] [[Google Scholar](#)]
8. Mauthe M, Orhon I, Rocchi C, Zhou X, Luhr M, Hijlkema KJ. Chloroquine inhibits autophagic flux by decreasing autophagosome-lysosome fusion. *Autophagy*. 2018;14:1435–1455. doi: 10.1080/15548627.2018.1474314. [[PMC free article](#)] [[PubMed](#)] [[CrossRef](#)] [[Google Scholar](#)]
9. Vincent MJ, Bergeron E, Benjannet S, Erickson BR, Rollin PE, Ksiazek TG. Chloroquine is a potent inhibitor of SARS coronavirus infection and spread. *Virology*. 2005;2:69. doi: 10.1186/1743-422X-2-69. [[PMC free article](#)] [[PubMed](#)] [[CrossRef](#)] [[Google Scholar](#)]
10. Fantini J, Di Scala C, Chahinian H, Yahi N. Structural and molecular modeling studies reveal a new mechanism of action of chloroquine and hydroxychloroquine against SARS-CoV-2 infection. *Int J Antimicrob Agents*. 2020;Apr 3 doi: 10.1016/j.ijantimicag.2020.105960. [[PMC free article](#)] [[PubMed](#)] [[CrossRef](#)] [[Google Scholar](#)]
11. Yan R, Zhang Y, Li Y, Xia L, Guo Y, Zhou Q. Structural basis for the recognition of the SARS-CoV-2 by full-length human ACE2. *Science*. 2020;367:1444–1448. doi: 10.1126/science.abb2762. [[PMC free article](#)] [[PubMed](#)] [[CrossRef](#)] [[Google Scholar](#)]
12. Matrosovich M, Herrler G, Klenk HD. Sialic acid receptors of viruses. *Top Curr Chem*. 2015;367:1–28. doi: 10.1007/128_2013_466. [[PMC free article](#)] [[PubMed](#)] [[CrossRef](#)] [[Google Scholar](#)]
13. Li W, Hulswit RJG, Widjaja I, Raj VS, McBride R, Peng W. Identification of sialic acid-binding function for the Middle East respiratory syndrome coronavirus spike glycoprotein. *Proc Natl Acad Sci USA*. 2017;114:E8508–E8517. doi: 10.1073/pnas.1712592114. [[PMC free article](#)] [[PubMed](#)] [[CrossRef](#)] [[Google Scholar](#)]
14. Park YJ, Walls AC, Wang Z, Sauer MM, Li W, Tortorici MA. Structures of MERS-CoV spike

- glycoprotein in complex with sialoside attachment receptors. *Nat Struct Mol Biol.* 2019;26:1151–1157. doi: 10.1038/s41594-019-0334-7. [[PMC free article](#)] [[PubMed](#)] [[CrossRef](#)] [[Google Scholar](#)]
15. Glende J, Schwegmann-Wessels C, Al-Falah M, Pfefferle S, Qu X, Deng H. Importance of cholesterol-rich membrane microdomains in the interaction of the S protein of SARS-coronavirus with the cellular receptor angiotensin-converting enzyme 2. *Virology.* 2008;381:215–221. doi: 10.1016/j.virol.2008.08.026. [[PMC free article](#)] [[PubMed](#)] [[CrossRef](#)] [[Google Scholar](#)]
16. Flores A, Ramirez-Franco J, Desplantes R, Debreux K, Ferracci G, Wernert F. Gangliosides interact with synaptotagmin to form the high-affinity receptor complex for botulinum neurotoxin B. *Proc Natl Acad Sci USA.* 2019;116:18098–18108. doi: 10.1073/pnas.1908051116. [[PMC free article](#)] [[PubMed](#)] [[CrossRef](#)] [[Google Scholar](#)]
17. Yahi N, Fantini J. Deciphering the glycolipid code of Alzheimer's and Parkinson's amyloid proteins allowed the creation of a universal ganglioside-binding peptide. *PLoS One.* 2014;9 doi: 10.1371/journal.pone.0104751. [[PMC free article](#)] [[PubMed](#)] [[CrossRef](#)] [[Google Scholar](#)]
18. Fantini J, Di Scala C, Evans LS, Williamson PT, Barrantes FJ. A mirror code for protein-cholesterol interactions in the two leaflets of biological membranes. *Sci Rep.* 2016;6:21907. doi: 10.1038/srep21907. [[PMC free article](#)] [[PubMed](#)] [[CrossRef](#)] [[Google Scholar](#)]
19. Fantini J, Carlus D, Yahi N. The fusogenic tilted peptide (67-78) of α -synuclein is a cholesterol binding domain. *Biochim Biophys Acta.* 2011;1808:2343–2351. doi: 10.1016/j.bbamem.2011.06.017. [[PubMed](#)] [[CrossRef](#)] [[Google Scholar](#)]
20. Wrapp D, Wang N, Corbett KS, Goldsmith JA, Hsieh CL, Abiona O. Cryo-EM structure of the 2019-nCoV spike in the prefusion conformation. *Science.* 2020;367:1260–1263. doi: 10.1126/science.abb2507. [[PMC free article](#)] [[PubMed](#)] [[CrossRef](#)] [[Google Scholar](#)]
21. Huta BP, Mehlenbacher MR, Nie Y, Lai X, Zubieta C, Bou-Abdallah F. The lysosomal protein saposin B binds chloroquine. *Chem Med Chem.* 2016;11:277–282. doi: 10.1002/cmdc.201500494. [[PMC free article](#)] [[PubMed](#)] [[CrossRef](#)] [[Google Scholar](#)]
22. Pawlowski AC, Stogios PJ, Koteva K, Skarina T, Evdokimova E, Savchenko A. The evolution of substrate discrimination in macrolide antibiotic resistance enzymes. *Nat Commun.* 2018;9 doi: 10.1038/s41467-017-02680-0. 112-112. [[PMC free article](#)] [[PubMed](#)] [[CrossRef](#)] [[Google Scholar](#)]
23. Di Scala C, Fantini J. Hybrid in silico/in vitro approaches for the identification of functional cholesterol-binding domains in membrane proteins. *Methods Mol Biol.* 2017;1583:7–19. doi: 10.1007/978-1-4939-6875-6_2. [[PubMed](#)] [[CrossRef](#)] [[Google Scholar](#)]
24. Lee J, Patel DS, Stähle J, Park SJ, Kern NR, Kim S. CHARMM-GUI membrane builder for complex biological membrane simulations with glycolipids and lipoglycans. *J Chem Theory Comput.* 2019;15:775–786. doi: 10.1021/acs.jctc.8b01066. [[PubMed](#)] [[CrossRef](#)] [[Google Scholar](#)]
25. Hollingsworth SA, Dror RO. Molecular dynamics simulation for all. *Neuron.* 2018;99:1129–1143. doi: 10.1016/j.neuron.2018.08.011. [[PMC free article](#)] [[PubMed](#)] [[CrossRef](#)] [[Google Scholar](#)]
26. Verma DK, Gupta D, Lal SK. Host lipid rafts play a major role in binding and endocytosis of influenza A virus. *Viruses.* 2018;10(11):650. doi: 10.3390/v10110650. [[PMC free article](#)] [[PubMed](#)] [[CrossRef](#)] [[Google Scholar](#)]
27. Lu Y, Liu DX, Tam JP. Lipid rafts are involved in SARS-CoV entry into Vero E6 cells. *Biochem Biophys Res Commun.* 2008;369:344–349. doi: 10.1016/j.bbrc.2008.02.023. [[PMC free article](#)] [[PubMed](#)] [[CrossRef](#)] [[Google Scholar](#)]
28. Fantini J, Yahi N. Elsevier Academic Press; San Francisco: 2015. Brain lipids in synaptic function and neurological disease. clues to innovative therapeutic strategies for brain disorders. ISBN: 9780128001110. [[Google Scholar](#)]
29. Hammache D, Piéroni G, Yahi N, Delézay O, Koch N, Lafont H. Specific interaction of HIV-1 and

- HIV-2 surface envelope glycoproteins with monolayers of galactosylceramide and ganglioside GM3. *J Biol Chem.* 1998;14:7967–7971. doi: 10.1074/jbc.273.14.7967. [[PubMed](#)] [[CrossRef](#)] [[Google Scholar](#)]
30. Fantini J, Garmy N, Mahfoud R, Yahi N. Lipid rafts: structure, function and role in HIV, Alzheimer's and prion diseases. *Expert Rev Mol Med.* 2002;4:1–22. doi: 10.1017/S1462399402005392. [[PubMed](#)] [[CrossRef](#)] [[Google Scholar](#)]
31. Berntsson RP, Peng L, Dong M, Stenmark P. Structure of dual receptor binding to botulinum neurotoxin B. *Nat Commun.* 2013;4:2058. doi: 10.1038/ncomms3058. [[PMC free article](#)] [[PubMed](#)] [[CrossRef](#)] [[Google Scholar](#)]
32. Fantini J, Yahi N, Garmy N. Cholesterol accelerates the binding of Alzheimer's β -amyloid peptide to ganglioside GM1 through a universal hydrogen-bond-dependent sterol tuning of glycolipid conformation. *Front Physiol.* 2013;4:120. doi: 10.3389/fphys.2013.00120. [[PMC free article](#)] [[PubMed](#)] [[CrossRef](#)] [[Google Scholar](#)]
33. Di Scala C, Yahi N, Boutemour S, Flores A, Rodriguez L, Chahinian H. Common molecular mechanism of amyloid pore formation by Alzheimer's β -amyloid peptide and α -synuclein. *Sci Rep.* 2016;6:28781. doi: 10.1038/srep28781. [[PMC free article](#)] [[PubMed](#)] [[CrossRef](#)] [[Google Scholar](#)]
34. Colson P, Rolain JM, Lagier JC, Brouqui P, Raoult D. Chloroquine and hydroxychloroquine as available weapons to fight COVID-19. *Int J Antimicrob Agents.* 2020;4 doi: 10.1016/j.ijantimicag.2020.105932. [[PMC free article](#)] [[PubMed](#)] [[CrossRef](#)] [[Google Scholar](#)]
35. Ponticelli C, Moroni G. Hydroxychloroquine in systemic lupus erythematosus (SLE) *Expert Opin Drug Saf.* 2017;16:411–419. doi: 10.1080/14740338.2017.1269168. [[PubMed](#)] [[CrossRef](#)] [[Google Scholar](#)]
36. Schrezenmeier E, Dörner T. Mechanisms of action of hydroxychloroquine and chloroquine: implications for rheumatology. *Nat Rev Rheumatol.* 2020;16:155–166. doi: 10.1038/s41584-020-0372-x. [[PubMed](#)] [[CrossRef](#)] [[Google Scholar](#)]
37. Zeballos RS, Fox RI, Cheresch DA, McPherson RA. Anti-glycosphingolipid autoantibodies in rheumatologic disorders. *J Clin Lab Anal.* 1994;8:378–384. doi: 10.1002/jcla.1860080607. [[PubMed](#)] [[CrossRef](#)] [[Google Scholar](#)]
38. McDonald G, Deepak S, Miguel L, Hall CJ, Isenberg DA, Magee AI. Normalizing glycosphingolipids restores function in CD4+ T cells from lupus patients. *J Clin Invest.* 2014;124:712–724. doi: 10.1172/JCI69571. [[PMC free article](#)] [[PubMed](#)] [[CrossRef](#)] [[Google Scholar](#)]
39. Hammache D, Yahi N, Maresca M, Piéroni G, Fantini J. Human erythrocyte glycosphingolipids as alternative cofactors for human immunodeficiency virus type 1 (HIV-1) entry: evidence for CD4-induced interactions between HIV-1 gp120 and reconstituted membrane microdomains of glycosphingolipids (Gb3 and GM3) *J Virol.* 1999;73:5244–5248. PMID: 10233996. [[PMC free article](#)] [[PubMed](#)] [[Google Scholar](#)]
40. Neu U, Woellner K, Gauglitz G, Stehle T. Structural basis of GM1 ganglioside recognition by simian virus 40. *Proc Natl Acad Sci USA.* 2008;105:5219–5224. doi: 10.1073/pnas.0710301105. [[PMC free article](#)] [[PubMed](#)] [[CrossRef](#)] [[Google Scholar](#)]